Strong electron-phonon coupling in the σ band of graphene

Federico Mazzola,[1] Thomas Frederiksen,[2,3] Thiagarajan Balasubramanian,[4] Philip Hofmann,[5]
Bo Hellsing,[2,6] and Justin W. Wells[1,*]

[1]*Department of Physics, Norwegian University of Science and Technology (NTNU), N-7491 Trondheim, Norway*
[2]*Donostia International Physics Center (DIPC) — UPV/EHU, E-20018 San Sebastián, Spain*
[3]*IKERBASQUE, Basque Foundation for Science, E-48013, Bilbao, Spain*
[4]*MAX IV Laboratory, PO Box 118, S-22100 Lund, Sweden*
[5]*Department of Physics and Astronomy, Interdisciplinary Nanoscience Center (iNANO), Aarhus University, Denmark*
[6]*Material and Surface Theory Group, Department of Physics, University of Gothenburg, Sweden*
(Received 5 July 2016; revised manuscript received 18 October 2016; published 24 February 2017)

First-principles studies of the electron-phonon coupling in graphene predict a high coupling strength for the σ band with λ values of up to 0.9. Near the top of the σ band, λ is found to be ≈ 0.7. This value is consistent with the recently observed kinks in the σ band dispersion by angle-resolved photoemission. While the photoemission intensity from the σ band is strongly influenced by matrix elements due to sublattice interference, these effects differ significantly for data taken in the first and neighboring Brillouin zones. This can be exploited to disentangle the influence of matrix elements and electron-phonon coupling. A rigorous analysis of the experimentally determined complex self-energy using Kramers-Kronig transformations further supports the assignment of the observed kinks to strong electron-phonon coupling and yields a coupling constant of 0.6(1), in excellent agreement with the calculations.

DOI: 10.1103/PhysRevB.95.075430

I. INTRODUCTION

The electron-phonon coupling (EPC) in graphene has been the subject of numerous studies [1–5]. Most of the literature focuses on the EPC in the π band, as these states form the Fermi surface and the EPC thus directly affects the materials' transport properties [6–8]. EPC in the σ band can be expected to be stronger than in the π band for several reasons: the atomic orbital overlap for the σ bands is substantially stronger than for the π band and the σ bands will thus be more sensitive to a vibration-related change of the bond length. Also, the π band's EPC is quite special because of the vanishing density of states near the Dirac point and the accompanying phase space reduction. While the EPC in the σ band has no direct implication for the transport properties of graphene, similar physics plays an important role in the superconductivity of the related material MgB_2 [9].

While no theoretical investigations have so far been published on the EPC in the σ band, two recent angle-resolved photoemission (ARPES) studies come to entirely different conclusions based on very similar data. Mazzola *et al.* [10] have reported the observation of a kink feature near the top of the σ band and ascribed this to strong EPC with a mass enhancement parameter λ between 0.7 and 1, depending on the graphene system. Similar kinks are often observed near the Fermi level and not usually expected and at higher binding energy. To explain the presence of the kink, Mazzola *et al.* needed to assume that the EPC in the σ band is determined by scattering effects involving predominately other σ states. More recently, Jung *et al.* [11] have reported similar data but have interpreted the observed kink as a consequence of a sublattice interference (SLI) effects, which suppress the photoemission intensity near normal emission, without the need to invoke any EPC, i.e., essentially using $\lambda = 0$. The difference in these interpretations does not only leave the question of the EPC strength open, it is also interesting in connection with the observation of other controversial kinklike features at higher binding energy [12–14].

Here we present a calculation of the EPC in the σ band from *first principles*, yielding an energy-dependent coupling strength. The calculation gives detailed insight into the origin of the strong EPC. We also report new ARPES results that have not been taken in the first Brillouin zone (first BZ) near normal emission, as in the previous works, but in a neighboring Brillouin zone (NBZ), such that the SLI effects no longer suppress the emission from the top of the σ band, qualitatively illustrating that the kink is not caused by SLI. We further deduce the phonon induced electronic self-energy from the ARPES data and show, using Kramers-Kronig (KK) analysis, that the result is self-consistent and agrees with the theoretical prediction for the EPC.

II. CALCULATIONS

The calculations of the EPC constant λ were based on Kohn-Sham density functional theory using the implementation in SIESTA [16] together with INELASTICA [17] for the EPC[1]

*justin.wells@ntnu.no

[1]We performed supercell calculations with a 9×9 repetition of the primitive two-atom graphene cell ($N = 162$ atoms in total), using the PBE-GGA functional [41], a 400 Ry cutoff for the real-space grid, a SZ basis set with an 0.02 Ry energy shift for the cutoff radii, and a 4×4 k-point sampling in the self-consistency loop. The interatomic distance was 1.48 Å. Force constants and gradients of the Kohn-Sham Hamiltonian were computed from finite differences with an amplitude of 0.02 Å. ρ and λ were evaluated with a Gaussian smearing of 0.1 eV for the δ functions, a dense 18×18 $\mathbf{k}$ grid and Γ phonons (i.e., $3N - 3$ modes) for the shrunk Brillouin zone of the 9×9 supercell.

yielding the electronic band structure and the phonon dispersion relations [Figs. 1(a) and 1(b)] of graphene in agreement with previous results [18–20]. In the low-temperature limit, phonon absorption is suppressed and the Eliashberg function α^2F is written as

$$\alpha^2F^E_{n\mathbf{k}}(\omega) = \sum_{\nu\mathbf{q}}\sum_{n'} |g^\nu(n\mathbf{k},n'\mathbf{k}+\mathbf{q})|^2 \times\delta(\varepsilon_{n'\mathbf{k}+\mathbf{q}} - \varepsilon_{n\mathbf{k}} - \hbar\omega_{\nu\mathbf{q}})\delta(\hbar\omega - \hbar\omega_{\nu\mathbf{q}}), \quad (1)$$

where the summation includes all electron scattering events from states $\varepsilon_{n'\mathbf{k}+\mathbf{q}}$ into the photohole state $\varepsilon_{n\mathbf{k}}$ with emission of a phonon with an energy $\hbar\omega_{\nu\mathbf{q}}$, and mediated by the EPC matrix elements $g^\nu(n\mathbf{k},n'\mathbf{k}+\mathbf{q})$. The $\mathbf{q}$-resolved matrix elements were computed implementing a finite-difference scheme similar to those of Refs. [21–24]. The EPC parameter for the electronic state $n\mathbf{k}$ is defined as

$$\lambda_{n\mathbf{k}} = 2\int d\omega \frac{\alpha^2F^E_{n\mathbf{k}}(\omega)}{\omega}. \quad (2)$$

Note that here $\lambda_{n\mathbf{k}}$ is a quantity depending on the energy of the electronic state, it does not correspond to the mass enhancement parameter at the Fermi energy [25]. In view of the nearly isotropic band structure, we average $\lambda_{n\mathbf{k}}$ along the 2D constant energy contour $\varepsilon_{n\mathbf{k}} = \varepsilon$, and define separate contributions for the σ and π bands, i.e.,

$$\lambda_{\sigma(\pi)}(\varepsilon) \equiv \frac{2}{\rho_{\sigma(\pi)}(\varepsilon)} \sum_{\sigma(\pi)\mathbf{k}} \lambda_{\sigma(\pi)\mathbf{k}}\delta(\varepsilon - \varepsilon_{\sigma(\pi)\mathbf{k}}), \quad (3)$$

where $\rho_\sigma(\varepsilon)$ and $\rho_\pi(\varepsilon)$ are the density of states (DOS) of the σ and π bands, respectively. Figure 1(c) shows the calculation of these EPC parameters in the energy range corresponding to all occupied states. Near the Fermi energy the EPC is very small ($\lambda_\pi < 0.1$) and consistent with values of the order 0.1-0.3 reported for n- and p-doped graphene [1,26]. On the other hand, near the top of the σ band we find a large value $\lambda_\sigma \approx 0.7$. This confirms the expectation that the EPC is considerably stronger in the σ band than in the π band.

To gain insight into the origin of the strong EPC in the σ band we computed the $\mathbf{q}$-resolved matrix elements for the longitudinal (LO) and transverse (TO) optical modes for electrons scattered from the σ-band maximum to either the inner or outer σ band. As shown in Fig. 1(d), for the considered $\mathbf{q}$ range the matrix elements are nearly constant with a magnitude of $|g^\nu| \approx 0.6$ eV for both modes and final states. At the onset of phonon emission the LO and TO contribution for a photohole in one of the σ bands can thus be estimated as $\lambda_\sigma \approx \sum_{\nu=\mathrm{LO,TO}} |g^\nu|^2/\hbar\omega_\nu(\rho_\sigma/2) = 2\times 0.6^2/0.2\times 0.15 = 0.54$, i.e., LO and TO are the primary modes responsible for a strong EPC.

III. MEASUREMENTS

Previously reported ARPES results for the σ band [10,11] were taken near normal emission, in the first BZ of graphene, and revealed a pronounced kink near the band maximum. In this geometry, the interference involving the two atoms in the unit cell of graphene leads to a strong suppression of the photoemission intensity near the top of the σ band [27] and for bands purely comprised of s-states [28]. While the observation of a kink near the band maximum was not disputed, its origin was: Mazzola *et al.* [10] ascribed the kink to strong EPC.

The sudden increase in the electron DOS could play a role equivalent to the Fermi-Dirac function cutoff at the Fermi level, hence reproducing the same physics at higher binding energies [10]. For a photohole created near the top of the sigma band, this is expected particularly if the intra σ band scattering dominates. The above estimate of λ_σ clearly indicates that this is the case.

Jung *et al.* [11] showed that the intensity of the two σ subbands near $\bar{\Gamma}$ is strongly anisotropic, something that they argued could potentially lead to a kink induced by "switching" the photoemission intensity from one subband to another. A spectral function based on the SLI, however, could not fit the data without the additional *ad hoc* assumption of a strong change of the state's photoemission cross section over a small k or energy range.

The ARPES experiments reported here (performed on the same graphene-on-SiC sample described previously [10,29]) avoid the complication of the vanishing intensity near the σ band top by taking data in the NBZ where no such total suppression occurs (for a calculation of the matrix elements see the supplementary information [15]). ARPES experiments were carried out at the beamline I4 MAX-lab, Lund, Sweden [30], using linear-horizontal light polarization. The sample temperature was 100 K. The energy and momentum resolutions were better than 35 meV and 0.018 Å^{-1}, respectively.

Figure 2 illustrates the effect of collecting data in different geometries on the observation of the kink. Figures 2(a)–2(e) and 2(f)–2(j) show the situation in the first BZ and the NBZ, respectively, while Figs. 2(a) and 2(f) display a model spectral function for the σ band maximum based on a simple first nearest-neighbors tight-binding calculation [15]. The images are identical, as this initial state dispersion is obviously periodic in reciprocal space. The striking role of the matrix elements becomes evident in Figs. 2(b) and 2(g), which show the expected photoemission intensities, calculated using Eqs. (1) and (2) from Ref. [11] for the matrix elements $M^\mathbf{k}$ and the photoemision intensity, respectively, with energy-independent photoionization cross sections $A_s = 0.5A_p$ for the first BZ ($h\nu = 36$ eV), and $A_s = 1.5A_p$ for the NBZ ($h\nu = 75$ eV) [31]. In the first BZ, the photoemission intensity is totally suppressed near $\bar{\Gamma}$ but in the NBZ it is not. Note that this simulation does not show any kinks, despite of the inclusion of SLI via the matrix elements. The effect of strong EPC is probed in Figs. 2(c), 2(h) and 2(d), 2(i). In 2(c) and 2(h), the expected photoemission intensity is shown for $\lambda = 0.7$ (calculated using a similar procedure as in Ref. [10] and further described in Ref. [15]) but the interference effects are switched off by setting the matrix elements $M^\mathbf{k} = 1$. The strong kink is evident. Figures 2(d) and 2(i) show the same calculation without artificially holding $M^\mathbf{k} = 1$, thus the interference effect is recovered. In the first BZ, the intensity is missing in the center of the image but the kink is still evident. In the NBZ, the full dispersion including kink is visible. Figures 2(e) and 2(j) show the corresponding experimental data which is in excellent agreement with Figs. 2(d) and 2(i). This shows that the kink cannot be explained by SLI without EPC.

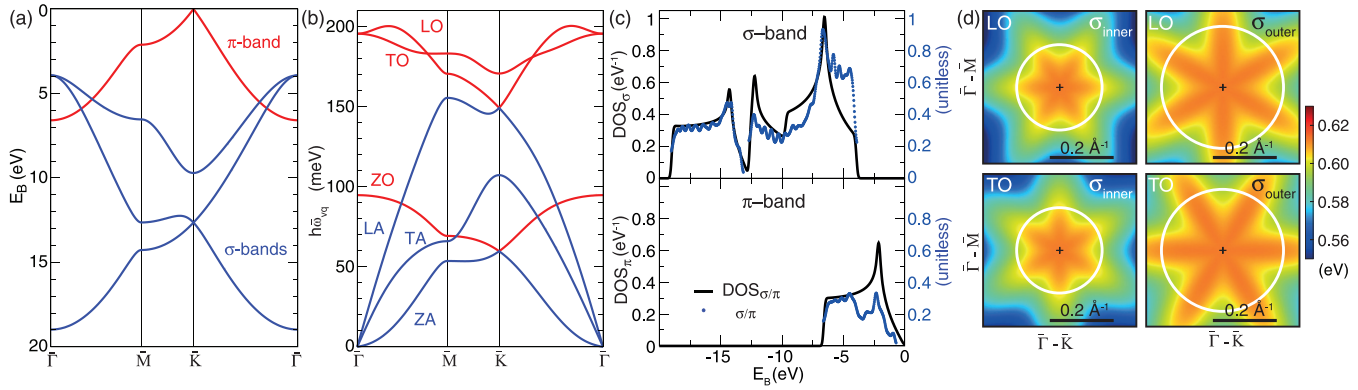

FIG. 1. (a) Electronic band structure of graphene with the π (σ) bands in red (blue). (b) Phonon band structure of graphene. The optical (acoustic) bands are shown by red (blue) lines. (c) Electronic DOS (black lines) and EPC strength $\lambda_{\sigma/\pi}$ (blue points) for a photohole generated in either a σ band (top) or π band (bottom). Near the top of the σ band $\lambda_\sigma \approx 0.7$. (d) Anisotropic momentum-resolved EPC matrix elements $|g^\nu(\mathbf{q})|$ for the LO and TO modes for electrons scattered from any of the two degenerate σ states at $\bar{\Gamma}$ (black cross) to either the inner or the outer σ band. White circles of radius 0.14 (0.20) Å^{-1} indicate states 200 meV below the σ-band maximum, i.e., final states that satisfy energy conservation. The weak anisotropy cancels out if one considers the sum over LO and TO modes as shown in Fig. S1 [15].

While the matrix elements do not suppress the photoemission intensity near the top of the σ band in the NBZ, the intensity of the two subbands still remains unequal. Calculations of this are shown in Figs. 2(k) and 2(l) for the first BZ and NBZ, respectively. The first BZ results agree with Ref. [11]. The NBZ results show a twofold symmetry with a much larger overlap between the subbands for certain angles. The results agree well with the experimental angular distribution in the NBZ shown in Fig. 2(m) [15].

IV. SELF-ENERGY ANALYSIS AND DISCUSSION

The highly anisotropic matrix elements in the first BZ and the possibility to suppress one of the subbands completely can be exploited for a more quantitative analysis of the EPC because it removes the difficulty of fitting two bands. We use this for an alternative proof that the kink is caused by EPC by extracting the bare band dispersion along with the real and imaginary parts of the electronic self-energy, $\Re\Sigma$ and $\Im\Sigma$.

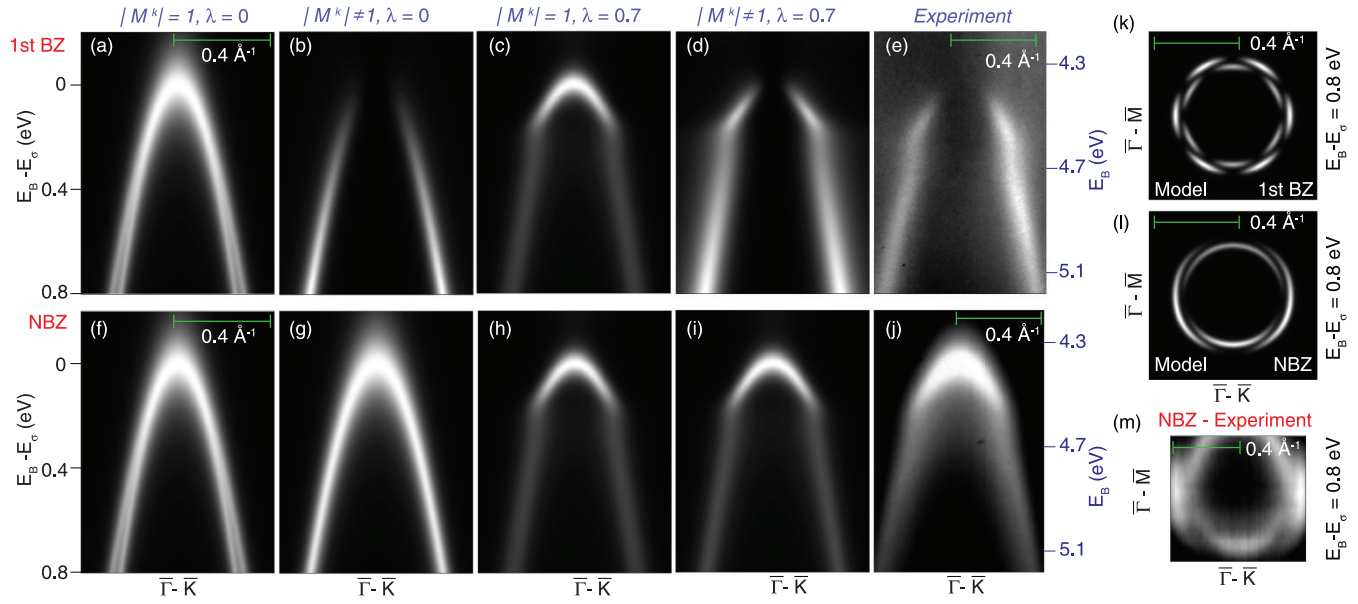

FIG. 2. Effect of SLI and EPC near the top of the σ band. The left axis ($E_B - E_\sigma$) indicates binding energy relative to the top of the σ band. The right (blue) axis indicates absolute binding energy. (a)–(e) Spectra relative to the first Brillouin zone (first BZ) center. (f)–(j) Spectra relative to the center of the first neighboring Brillouin zone (NBZ). (a) and (f) Spectral function determined using a tight-binding approach and a constant $\Im\Sigma$ (with $\Re\Sigma = 0$). (b) and (g) Expected ARPES intensity without EPC, i.e., spectral function times calculated matrix elements to account for SLI. (c) and (h) Expected ARPES intensity with EPC but without SLI. (d) and (i) Expected ARPES intensity including both EPC and SLI. (e) and (j) Measured ARPES intensities. (k) and (l) Calculated ARPES intensity at a constant energy below the band maximum in the first and neighboring BZs, respectively, not including EPC. (m) Experimental ARPES intensity in the NBZ.

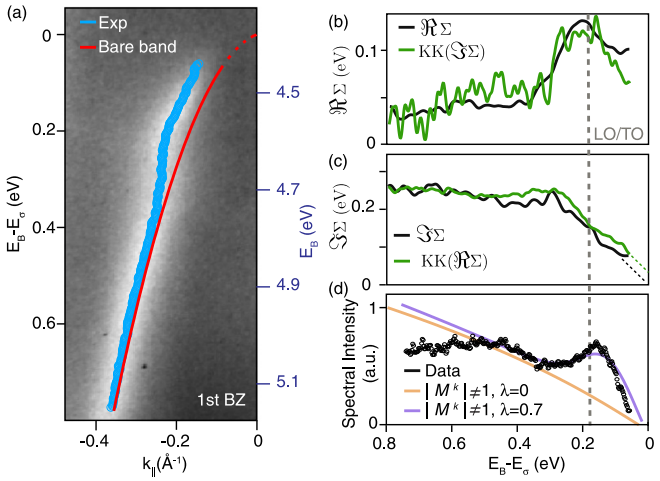

FIG. 3. Analysis of the real and imaginary parts of the quasiparticle self-energy, $\Re\Sigma$ and $\Im\Sigma$. (a) ARPES data with the bare band and experimentally determined dispersion. The left axis ($E_B - E_\sigma$) indicates binding energy relative to the top of the σ band. The right (blue) axis indicates absolute binding energy. (b) $\Re\Sigma$ (black) plotted alongside the KK-transformed $\Im\Sigma$ (green); (c) $\Im\Sigma$ (black), alongside the KK-transformed $\Re\Sigma$ (green). (d) Comparison between the calculated and experimentally determined spectral intensity (i.e., MDC peak height) as function binding energy: the black curve is extracted from the experiment (a), the yellow curve from a simulated spectrum with inclusion of SLI, but zero EPC and the purple curve is extracted from a simulated spectrum with inclusion of both SLI and EPC.

In principle, $\Re\Sigma$ and $\Im\Sigma$ can be determined independently from the measured spectral function but only when the bare band dispersion is known [32]. Using a tight-binding model for this is not an adequate approach, since the parameters are not known with sufficient accuracy. We instead use the self-consistent method proposed by Pletikosić *et al.* [33] to extract the bare band dispersion, $\Re\Sigma$ and $\Im\Sigma$. Figure 3(a) gives the ARPES data in the first BZ with the bare band dispersion (red) and the experimentally determined dispersion from momentum distribution curve (MDC) analysis (blue). $\Re\Sigma$ is extracted from the experimentally determined dispersion relative to the bare band (i.e., the renormalization) and plotted in black in Fig. 3(b). $\Im\Sigma$ is extracted from the MDC linewidth and plotted in black in Fig. 3(c). The kink is particularly well seen in $\Re\Sigma$. In order to confirm that the kink is due to EPC, we KK transform both $\Re\Sigma$ and $\Im\Sigma$ referred to as KK($\Re\Sigma$) and KK($\Im\Sigma$), respectively, and plot the results in green in Figs. 3(c) and 3(b), respectively. KK transformations have been performed under the criteria discussed in Ref. [33], In addition, the high-energy tails of $\Re\Sigma$, $\Im\Sigma$, and E_B are not affected by the finite energy range of the ARPES acquisition. The similarity of $\Re\Sigma$ with KK($\Im\Sigma$) and $\Im\Sigma$ with KK($\Re\Sigma$) is striking. In all cases, it is also clear that the binding energy of the kink is at $\approx$200 meV below the σ-band maximum, consistent with predominant coupling to LO and TO phonons. This analysis yields an EPC strength of $\lambda \approx 0.6$, which is extracted following the method described in Refs. [26,33] and is consistent with the calculated values.

Finally, we emphasize that the results here can be viewed to be consistent with those of Jung *et al.* [11]. The experimental data are very similar and the authors, after introducing the SLI effect, find that the spectral function cannot be fitted within this model without the *ad hoc* assumption of a photoemission cross section A_s that is strongly k-dependent (or, equivalently, energy-dependent), so as to give rise to a "singularity" in $M^{\mathbf{k}}$ at the location of the kink (as shown in Fig. 4(a) of Ref. [11]). In the presence of EPC, such assumptions are not necessary because the EPC anyway acts to redistribute the spectral intensity: near the top of the band, the increased lifetime of the photohole leads to narrower MDCs with higher peak intensity values. Figure 3(d) shows the experimentally determined intensity peak height (each MDC is fitted with a Voigt function, from which the peak height is found) alongside the peak height calculated both with and without EPC [extracted from Figs. 2(d) and 2(b), respectively]. Ignoring EPC gives rise to a spectral intensity which is smoothly increasing from zero at the energy of the band maximum, whereas the inclusion of EPC gives rise to a spectral intensity which is peaked at an energy $\approx$170 meV from the band maximum (corresponding to the energy of the LO/TO phonons).

V. CONCLUSION

In conclusion, we have investigated the role and strength of the controversial EPC in the σ band of graphene and provide relevant and complementary ARPES measurements to elucidate the origin of the observed band-dispersion "kinks." DFT-based calculations for the EPC constant λ in the whole energy range of occupied bands are presented, showing λ values up to 0.9 in the σ band. The theoretical prediction of $\lambda_\sigma = 0.7$ near the band maximum is in excellent agreement with our experimental ARPES data and shown to originate primarily from the LO and TO phonons.

Although the σ band lies far from the Fermi level and does not contribute to graphene's transport properties, it is interesting to speculate what would happen if the σ band could be shifted to the Fermi level: using the McMillan formula [34] (corrected by Allen *et al.* [35], and valid for $\lambda < 1.5$),

$$T_c = \frac{\hbar\omega_{\log}}{1.20}\exp\left(-\frac{1.04(1+\lambda)}{\lambda-\mu^*(1+0.62\lambda)}\right), \tag{4}$$

it is possible to relate λ to the superconducting critical temperature T_c. Assuming a value of the effective Coulomb repulsion $\mu^* = 0.1$, as is conventional for s and p band superconductors [36], the logarithmically averaged phonon frequency $\omega_{\log} = 725.9$ cm^{-1} (equivalent to 1035.77 K) [37] and $0.8 < \lambda < 1.0$, we predict 49 K $< T_c <$ 72 K.

We acknowledge that this estimate is purely speculative; a shift of $\approx$4 eV is beyond the means of conventional doping, and would presumably require such a high degree ($\approx$ 50%) of substitution that the material could no longer be considered to be graphene. On the other hand, it is interesting to contribute to the hypothesis that superconducting graphene-derived 2D materials may exist [38,39]. Finally, it is also worth noticing that similar physics was already found in the related material, MgB_2 ($T_c = 39$ K) [40], in which the B atoms form a graphenelike structure. In this case, one finds a similar σ band structure and a similar EPC coupling strength [9], thus adding support for the existence of graphene-derived σ band superconductors.

We have also shown that the SLI phenomenon has no relevance for the kink observed in ARPES, even though it influences the total intensity and the visibility of the two σ subbands. The SLI-induced total suppression of a given subband in the first BZ can even be used for a quantitative analysis of the self-energy Σ, which shows a consistent picture that the kink is indeed caused by strong EPC.

ACKNOWLEDGMENTS

We thank Rositsa Yakimova for supplying the sample and Keun Su Kim, Kai Rossnagel, Mads Brandbyge, Tue Gunst, and Antti-Pekka Jauho for helpful discussions. We gratefully acknowledge funding from VILLUM FONDEN via the Centre of Excellence for Dirac Materials (Grant No. 11744), Aarhus University Research Foundation, the Danish Council for Independent Research, Natural Sciences under the Sapere Aude program (Grant No. DFF-4002-00029), Center for Nanostructured Graphene (Project DNRF58), the Basque Departamento de Educación and the UPV/EHU (Grant No. IT-756-13), the Spanish Ministerio de Economía y Competitividad (Grant No. MAT2013-46593-C6-2-P), the European Union FP7-ICT project PAMS (Contract No. 610446) and the Research Council of Norway through Project No. 250555 "GraSeRaD" in the *Nano2021* program.

[1] M. Calandra and F. Mauri, Phys. Rev. B **76**, 205411 (2007).
[2] C.-H. Park, F. Giustino, M. L. Cohen, and S. G. Louie, Nano Lett. **8**, 4229 (2008).
[3] S. Ulstrup, M. Bianchi, R. Hatch, D. Guan, A. Baraldi, D. Alfè, L. Hornekær, and P. Hofmann, Phys. Rev. B **86**, 161402 (2012).
[4] M. Bianchi, E. D. L. Rienks, S. Lizzit, A. Baraldi, R. Balog, L. Hornekær, and P. Hofmann, Phys. Rev. B **81**, 041403 (2010).
[5] A. V. Fedorov, N. I. Verbitskiy, D. Haberer, C. Struzzi, L. Petaccia, D. Usachov, O. Y. Vilkov, D. V. Vyalikh, J. Fink, M. Knupfer, B. Büchner, and A. Grüneis, Nat. Commun. **5**, 3257 (2014).
[6] G. Grimvall, *The Electron-Phonon Interaction in Metals* (North-Holland, Amsterdam, 1981).
[7] B. Hellsing, A. Eiguren, and E. V. Chulkov, J. Phys. Condens. Matter **14**, 5959 (2002).
[8] P. Hofmann, I. Y. Sklyadneva, E. D. L. Rienks, and E. V. Chulkov, New J. Phys. **11**, 125005 (2009).
[9] H. Choi, D. Roundy, H. Sun, M. Cohen, and S. Louie, Nature (London) **418**, 758 (2002).
[10] F. Mazzola, J. W. Wells, R. Yakimova, S. Ulstrup, J. A. Miwa, R. Balog, M. Bianchi, M. Leandersson, J. Adell, P. Hofmann, and T. Balasubramanian, Phys. Rev. Lett. **111**, 216806 (2013).
[11] S. W. Jung, W. J. Shin, J. Kim, L. Moreschini, H. W. Yeom, E. Rotenberg, A. Bostwick, and K. S. Kim, Phys. Rev. Lett. **116**, 186802 (2016).
[12] J. Graf, G.-H. Gweon, K. McElroy, S. Y. Zhou, C. Jozwiak, E. Rotenberg, A. Bill, T. Sasagawa, H. Eisaki, S. Uchida, H. Takagi, D.-H. Lee, and A. Lanzara, Phys. Rev. Lett. **98**, 067004 (2007).
[13] T. Valla, T. E. Kidd, W.-G. Yin, G. D. Gu, P. D. Johnson, Z.-H. Pan, and A. V. Fedorov, Phys. Rev. Lett. **98**, 167003 (2007).
[14] W. Zhang, G. Liu, J. Meng, L. Zhao, H. Liu, X. Dong, W. Lu, J. S. Wen, Z. J. Xu, G. D. Gu, T. Sasagawa, G. Wang, Y. Zhu, H. Zhang, Y. Zhou, X. Wang, Z. Zhao, C. Chen, Z. Xu, and X. J. Zhou, Phys. Rev. Lett. **101**, 017002 (2008).
[15] See Supplemental Material at http://link.aps.org/supplemental/10.1103/PhysRevB.95.075430 for details of the EPC simulation, the tight binding and spectral function calculations and for additional ARPES data collected at different azimuthal angles.
[16] J. M. Soler, E. Artacho, J. D. Gale, A. García, J. Junquera, P. Ordejón, and D. Sánchez-Portal, J. Phys. Condens. Matter **14**, 2745 (2002).
[17] T. Frederiksen, M. Paulsson, M. Brandbyge, and A.-P. Jauho, Phys. Rev. B **75**, 205413 (2007).
[18] L. Wirtz and A. Rubio, Solid State Commun. **131**, 141 (2004).
[19] J. Maultzsch, S. Reich, C. Thomsen, H. Requardt, and P. Ordejón, Phys. Rev. Lett. **92**, 075501 (2004).
[20] Y. Liu, L. Zhang, M. K. Brinkley, G. Bian, T. Miller, and T.-C. Chiang, Phys. Rev. Lett. **105**, 136804 (2010).
[21] F. Giustino, M. L. Cohen, and S. G. Louie, Phys. Rev. B **76**, 165108 (2007).
[22] K. Kaasbjerg, K. S. Thygesen, and K. W. Jacobsen, Phys. Rev. B **85**, 165440 (2012).
[23] K. Kaasbjerg, K. S. Thygesen, and K. W. Jacobsen, Phys. Rev. B **85**, 115317 (2012).
[24] T. Gunst, T. Markussen, K. Stokbro, and M. Brandbyge, Phys. Rev. B **93**, 035414 (2016).
[25] J. E. Gayone, S. V. Hoffmann, Z. Li, and P. Hofmann, Phys. Rev. Lett. **91**, 127601 (2003).
[26] J. C. Johannsen, S. Ulstrup, M. Bianchi, R. Hatch, D. Guan, F. Mazzola, L. Hornekær, F. Fromm, C. Raidel, T. Seyller, and P. Hofmann, J. Phys. Condens. Matter **25**, 094001 (2013).
[27] E. L. Shirley, L. J. Terminello, A. Santoni, and F. J. Himpsel, Phys. Rev. B **51**, 13614 (1995).
[28] S. Lizzit, G. Zampieri, L. Petaccia, R. Larciprete, P. Lacovig, E. D. L. Rienks, G. Bihlmayer, A. Baraldi, and P. Hofmann, Nat. Phys. **6**, 345 (2010).
[29] F. Mazzola, T. Trinh, S. Cooil, E. R. Østli, K. Høydalsvik, E. T. B. Skjønsfjell, S. Kjelstrup, A. Preobrajenski, A. A. Cafolla, D. A. Evans, D. W. Breiby, and J. W. Wells, 2D Materials **2**, 025004 (2015).
[30] B. Jensen, S. Butorin, T. Kaurila, R. Nyholm, and L. Johansson, Nucl. Instrum. Methods Phys. Res., Sect. A **394**, 243 (1997).
[31] J. J. Yeh and I. Lindau, At. Data Nucl. Data Tables **32**, 1 (1985).
[32] J. Gayone, C. Kirkegaard, J. Wells, S. Hoffmann, Z. Li, and P. Hofmann, Appl. Phys. A **80**, 943 (2005).
[33] I. Pletikosić, M. Kralj, M. Milun, and P. Pervan, Phys. Rev. B **85**, 155447 (2012).
[34] W. L. McMillan, Phys. Rev. **167**, 331 (1968).
[35] P. B. Allen and R. C. Dynes, Phys. Rev. B **12**, 905 (1975).
[36] D. M. Gaitonde, P. Modak, R. S. Rao, and B. K. Godwal, Bull. Mater. Sci. **26**, 137 (2003).
[37] C. Si, Z. Liu, W. Duan, and F. Liu, Phys. Rev. Lett. **111**, 196802 (2013).
[38] G. Savini, A. C. Ferrari, and F. Giustino, Phys. Rev. Lett. **105**, 037002 (2010).
[39] M. Calandra and F. Mauri, Phys. Rev. Lett. **95**, 237002 (2005).
[40] J. M. An and W. E. Pickett, Phys. Rev. Lett. **86**, 4366 (2001).
[41] J. P. Perdew, K. Burke, and M. Ernzerhof, Phys. Rev. Lett. **77**, 3865 (1996).